Bone Reports 19 (2023) 101710

Contents lists available at ScienceDirect

Bone Reports

journal homepage: www.elsevier.com/locate/bonr

Bone strength is reduced in a neonatal androgenized rat model

Lady Katerine Serrano Mujica [a], Carolina dos Santos Amaral [b], Fernanda Soldatelli Valente [c], Ligia Gomes Miyazato [c], Soraia Macari [d], Tarcília Aparecida da Silva [d], Breno Rocha Barrioni [e], Bruna Leonel Carlos [f], Guilherme Jafroni Alves Silva [f], Antônio Carlos Shimano [f], Alfredo Quites Antoniazzi [b], Melissa Orlandin Premaor [g], Fabio Vasconcellos Comim [g,*]

[a] Animal Science Department, Cooperative University of Colombia (UCC), Bucaramanga, Colombia
[b] Laboratory of Biotechnology and Animal Reproduction - BioRep, Federal University of Santa Maria (UFSM), Santa Maria, Brazil
[c] Animal Care Facility, Federal University of Santa Maria (UFSM), Santa Maria, Brazil
[d] Department of Oral Pathology and Surgery, Faculty of Dentistry, Federal University of Minas Gerais (UFMG), Belo Horizonte, Minas Gerais, Brazil
[e] Department of Metallurgical and Materials Engineering, Faculty of Engineering, Federal University of Minas Gerais, Belo Horizonte (UFMG), Minas Gerais, Brazil
[f] Department of Biomechanics, Medicine and Locomotor Apparatus Rehabilitation, Faculty of Medicine, University of Sao Paulo (USP), Ribeirão Preto, São Paulo, Brazil
[g] Department of Clinical Medicine, Faculty of Medicine, Federal University of Minas Gerais (UFMG), Belo Horizonte, Brazil

ARTICLE INFO

Keywords:
Polycystic ovary syndrome
Bone
Animal models of PCOS
microCT
Mechanical test

ABSTRACT

Background: Whether polycystic ovary syndrome (PCOS) affects bone health during a woman's lifespan remains controversial. An androgenized rodent model replicated many metabolic and reproductive features of women with PCOS, and we aimed to use it to investigate the impact of androgens on microarchitecture (by micro-CT), bone mechanical strength, bone formation and resorption markers in rats with intact ovaries (SHAM) who underwent oophorectomy.

Methods: Wistar rats (*Rattus norvegicus albinus)* were employed for the experiments in this study. The protocol of androgenization consisted of the application of 1.25 mg s.c. testosterone propionate beteween days 2–5 of life, while the controls received the same amount of corn oil s.c. as previously established. Androgenized SHAM rats exhibited chronic anovulation identified by vaginal cytology and a reduction in the proportion of corpus luteum in the ovary in comparison to control SHAM rats. The realization of the ovariectomy or SHAM procedure occurred on Day 100 of life. All groups (n = 8) were followed-up for 180 days to address the study endpoints.

Results: Micro-CT from androgenized female rats (SHAM) showed a divergence between the trabecular and cortical bone profiles. Compared to SHAM controls, these rats had an increase in trabecular bone mass with a diminution in bone resorption C-terminal telopeptide of type 1 collagen (CTX) ($p < 0.05$), a concomitant decrease in cortical area and thickness in the femur, and a reduction in the strength of the femur on the mechanical test ($p < 0.01$).

Conclusions: Our results suggest that a reduction in the cortical thickness and cortical area observed in PCOS model rats was associated with a reduced strength of the femur, despite increased trabecular formation. Ovariectomy in the androgenized OVX group limited the progression rate of cortical bone loss, resulting in bone resistance and cortical thickness comparable to those observed in the control OVX group.

1. Introduction

Polycystic ovary syndrome (PCOS) is the most common endocrine disorder in women (Teede et al., 2018; McCartney Ch and Marshall, 2016). Currently, the impact of PCOS on bone health is not clearly known. The available literature is discordant about the presence of lower bone mass (Sir-Petermann et al., 2016; Piovezan et al., 2019; Rubin et al., 2016; Yang et al., 2018; Schmidt et al., 2012) or the incidence of bone fractures in women with PCOS, as the relative risk of fractures is described as reduced or elevated (Kassanos et al., 2010; Katulski et al., 2014; Karadag et al., 2017; Kalyan et al., 2017). This substantial divergence in results may be a product of several factors,

* Corresponding author at: Department of Clinical Medicine, Faculty of Medicine, Federal University of Minas Gerais, Av Prof. Alfredo Balena 190, room 246, Belo Horizonte, MG, Brazil.
E-mail address: fcomim@medicina.ufmg.br (F.V. Comim).

https://doi.org/10.1016/j.bonr.2023.101710
Received 10 June 2023; Received in revised form 29 July 2023; Accepted 17 August 2023

including age, BMI, hormonal treatment, and the presence of eating disorders, diabetes mellitus, and amenorrhea (Kalyan et al., 2017).

Animal models of PCOS have gained attention as a helpful tool to understand the mechanisms of the developmental course of PCOS (Stener-Victorin et al., 2020; Padmanabhan and Veiga-Lopez, 2013). In our study, we employed the previously described rat model of PCOS obtained from the injection of 1.25 mg of testosterone propionate on the second day of life. When these rats reach adulthood, they exhibit chronic anovulation, polycystic ovaries, hyperandrogenism and insulin resistance (Anzai et al., 2017; Marcondes et al., 2015; Serrano Mujica et al., 2021; Ota et al., 1983; Pinilla et al., 2002). Interestingly, these androgenized rats show at adult age, higher levels of serum luteinizing hormone (LH) and serum testosterone (T) than control rats (Anzai et al., 2017; Marcondes et al., 2015; Ota et al., 1983). The ovaries of these animals display a reduced number of corpora lutea (CL) (Marcondes et al., 2015; Ota et al., 1983) a higher area of theca-interstitial tissue, and increased expression of luteinizing hormone receptor (*Lhcgr*) and the cytochrome P450 (*Cyp17a1*), key players in the steroidogenic pathway (Anzai et al., 2017; Marcondes et al., 2015). There is also evidence of metabolic abnormalities, characterized by higher total, low-density lipoprotein cholesterol, triglycerides, TyG index, and the accumulation of lipids in the liver, related to insulin resistance (Anzai et al., 2017). A disruption of the REDOX state, represented by total oxidative status (TOS), and the ratio between total oxidative status and total antioxidant capacity (TOS/TAC) was also identified (Serrano Mujica et al., 2021).

To date, few studies have reported bone characteristics in animal models of PCOS. Together, these studies identified increased bone mass and trabecular mass in long bones, suggesting a favorable bone microarchitecture (Tamura et al., 2005; Turner et al., 1990; Mujica et al., 2021), but none have evaluated bone strength by mechanical testing. Similarly, no study has explored bone proprieties in an animal model of PCOS after oophorectomy (postmenopausal osteoporosis), which is one of the aims of the present study.

2. Methods

2.1. Ethical statement

This study was approved by the local Ethics Committee on Animal Use from Federal University of Santa Maria, Brazil (CEUA) under protocol number 1619180917 - (http://ceuaonline.ufsm.br/verificacao_code.php?ceua=1619180917&iddoc=0&id_resu=1980&id_par=1), in accordance with ARRIVE guidelines and national and institutional guidelines for animal welfare.

2.2. Animals and experimental protocol

2.2.1. General information

Overall, 38 female Wistar rats (*Rattus norvegicus albinus*) were employed for this experimental study. This number of rats was calculated to provide approximately eight animals per group based on an earlier study (Mujica et al., 2021). Androgenization consisted of the administration of a single subcutaneous (s.c.) injection of 1.25 mg testosterone propionate (Androgenol™) (androgenized group) or vehicle control −1.25 mg corn oil s.c. (control group) in pups at Days 2–5 of life (Anzai et al., 2017; Marcondes et al., 2015; Serrano Mujica et al., 2021; Ota et al., 1983). This neonatal protocol replicates several reproductive and metabolic features of PCOS (Anzai et al., 2017; Marcondes et al., 2015; Serrano Mujica et al., 2021; Ota et al., 1983; Pinilla et al., 2002). The allocation for a group of pups was aleatory, and the dams were kept with their pups until weaning (21 days); groups of androgenized and control pups remained in separated cages to avoid contamination with hormones excreted in the urine or feces. The rats were maintained at a temperature of 22 °C and 55 % to 65 % humidity under artificial illumination with a 12-h light/dark cycle; they received a standard pellet diet with water available ad libitum. Surgery (ovariectomy or SHAM procedure) was performed on Day 100 of life under general anesthesia (ketamine and isoflurane) associated with pre- and postsurgical analgesia with tramadol chloride (Tramadol™, Pfizer, Brazil) and ketoprofen (Ketofen, Merial, Brazil). Four groups were constituted in this study: 1) "Control OVX", (n = 9); 2) "Control SHAM" (n = 9); 3) "Androgenized OVX" (n = 10); and 4) "Androgenized SHAM" (n = 10).

2.2.2. Ovariectomy/SHAM procedures

At day 100 of life, sexually mature, and with a weight above 200 g, rats were submitted to the OVX or SHAM procedures which included in both cases, identification of the ovary and externalization, with removal of the ovaries in OVX group and preservation of the gonads in SHAM group. These surgeries were executed under general anesthesia induced by ketamine and isoflurane administration. In addition, tramadol chloride (Tramadol™, Pfizer, Sao Paolo, Brazil) and ketoprofen (Ketofen, Merial, Paulinia, Brazil) were used for pre-and postsurgical analgesia. Bilateral ovariectomy was realized through the dorsolateral approach. Under deep anesthesia, rats were put at a lateral position and both flanks were exposed, shaved, and cleaned with chlorhexidine. A scalpel incision was performed on the lateral side along a line spanning from the second to the fifth lumbar vertebra. After brief exploration, the ovary was located and removed. All plans were closed with 3–0 absorbable sutures. The same procedure was performed to the removal of the right and the left ovary. SHAM rats were submitted to the same anesthesia and surgery protocol (including localization of the ovary and externalization) but did not undergo ovariectomy. Animals were observed each 10 min after surgery to monitor the development of complications in the first hour and the 30 and 30 min until the fourth hour (Serrano Mujica et al., 2021). Successful oophorectomy was confirmed in all cases by the presence of undetectable levels of circulating estradiol using commercial electrochemiluminescent assays (Architect Estradiol, Abbot Laboratories, Wiesbaden, Germany – protocol available at https://www.ilexmedical.com/files/PDF/Estradiol_ARC.pdf) not observed in SHAM rats (Serrano Mujica et al., 2021; Monteiro et al., 2016). The evaluation of endpoints of interest (bone size, bone mechanical tests, bone microCT and bone metabolic parameters) were performed by blinded examiners who did not know the animal groups.

2.2.3. Euthanasia

All animals were euthanized at approximately Day 180 during metestrus/diestrous (Serrano Mujica et al., 2021). Animals were anesthetized with isoflurane plus intramuscular administration of tramadol chloride (Tramadol™, Pfizer) (20–40 mg/kg). Blood was collected and centrifuged at 40 °C and 5000 rpm/4696 g (Sorvall-Thermo Scientific, Asheville, USA) for 15 min and stored at −80 °C.

2.2.4. Bone analysis

2.2.4.1. Micro-CT (femur and spine). The structural properties of the trabecular and cortical bone from spine and femur were determined with a high-resolution micro-CT system (SkyScan 1172×, Aartselaar, Belgium). The images were acquired using an isotropic voxel size of 18 μm (50 kV aluminum filter, 0.5 mm, 0.5° rotation angle). Contour methods were used to delineate the region of interest to be analyzed as previously described (Monteiro et al., 2016). Reconstructions were executed with NRecon (v 1.6.9.8; Bruker micro-CT). Samples were previously prepared in 4 % paraformaldehyde for 24 h and then transferred to 70 % ethanol. The variables of interest obtained with micro-CT were 1) bone mineral density (BMD g/cm); 2) bone volume (BV mm); 3) bone volume/total volume ratio (BV/TV%); 4) trabecular thickness (Tb.Th mm); 5) trabecular number (Tb.n mm); 6) trabecular separation (Tb.sp. mm); and 7) the structure model index (SMI). The cortical bone was analyzed using the following variables: 1) Tt.Ar (total transverse area

within the periosteal envelope mm; 2) Ct.Ar (cortical area mm), 3)Tt.Ar/Ct.Ar (fraction of cortical area %); and 4) Ct.Th (cortical thickness mm). The lumbar rat spines were processed similarly to the femur and were scanned in the same equipment using the following parameters: energy/intensity: 70 kVp, 57 μA, 4 W; image matrix: 2048 × 2048 pixels; and voxel size: 20 μm. Segmentation thresholds of 190 and 280 and a Gaussian filter (σ = 0.8, support of one voxel) were used for image analysis. Trabecular variables obtained with micro-CT were 1) bone mineral density (BMD g/cm); 2) bone volume (BV mm); 3) bone volume/total volume ratio (BV/TV%); 4) trabecular thickness (Tb.Th mm); 5) trabecular number (Tb.n mm); 6) trabecular separation (Tb.sp. mm); and 7) the structure model index (SMI). All analyses were performed using CT Analyzer software (Skyscan Bruker®, Germany) (Monteiro et al., 2016).

2.2.4.2. Femur weight and size. Dissected femurs were weighed on a scale with 0.01 g precision (AC-2000, Marte®, Brazil). The femur length was measured with a digital caliper with 0.01 mm precision (Mitutoyo®, USA).

2.2.4.3. Mechanical test. The right femur of each rat was submitted to a bending test with a Universal Testing Machine (DL10.000, EMIC®, Brazil) from the Bioengineering Laboratory of FMRP/USP (Monteiro et al., 2016; Yanagihara et al., 2015). The proximal femur was wrapped in saline soaked cotton to avoid heating the region to be evaluated during polymerization of the polimetacrilate/Metilmetacrilate EDMA (Crosslink) DMT (AutoCril, IMODONTO, Brazil) (Underlying data: Supplemental Fig. 1). After that, they were submitted to a 50 kg/force load cell; the force was applied at a speed of 1 mm/min until sample rupture of the femur neck. The accommodation time was 20 s. The properties analyzed were maximum strength and relative stiffness (Yanagihara et al., 2015).

2.2.5. Biochemical and hormonal data

2.2.5.1. Enzyme-linked immunosorbent assay (ELISA). The cross-linked C-telopeptide of type I collagen (CTX) levels and Procollagen I N-terminal propeptide (PINP) (both with a coefficient of variation <10 %) were measured in serum at a single occasion using a specific rat ELISA (Cloud Clone Corp, USA) according to the manufacturer's protocols. The assay for cross-linked C-telopeptide of type I collagen (CTX) (Cloud Clone Corp, USA - Code CEA665Ra) was based on a competitive inhibition (http://www.cloud-clone.com/products/CEA665Ra.html) while the Procollagen I N-terminal propeptide (PINP) Cloud Clone Corp, (USA - Code SEA957Ra) was based on a double-antibody sandwich assay (http://www.cloud-clone.com/products/SEA957Ra.html).

2.2.6. Ovarian histology

At Day 180, after euthanasia, rat ovaries were immediately fixed in 4 % paraformaldehyde for 24 h. After that, these ovaries were processed by the following steps: alcohol dehydration, diaphanization in xylene, liquid Paraplast™ (Sigma, Brazil), impregnation in a drying stove at 60 °C, and Para-plast™ inclusion at room temperature. Sections of 5 mm thickness on glass slides were obtained using a microtome (RM2335, Leica Biosystems). The slides were stained with hematoxylin and eosin. The morphological and morphometric analyses (follicle and corpora lutea counting) used an optical microscope (Leica, DMI4000B) adjusting the magnification to allow identification of structures (e.g., healthy and atretic follicles and the corpus luteum) (Serrano Mujica et al., 2017; Sun et al., 2013).

2.2.7. Vaginal smear cytology

Vaginal smears were collected on glass slides to evaluate the animal's estrus cycles from 60 days to 71 days of age. Pancotico™ (Laborclin, Brazil) staining was used to analyze the vaginal cytology. Cytology was examined by a blinded examiner (LKSM) with experience in this procedure. A normal estrus cycle was defined as exhibiting all phases (proestrus, estrus, metestrus, and diestrus) over a period of 4 and 5 days, as previously characterized in the literature (Serrano Mujica et al., 2017; Sun et al., 2013).

2.2.8. Osteoclast and osteoblast number

Histology analysis was performed as previously described (Macari et al., 2015; Montalvany-Antonucci et al., 2018). Bone samples were fixed in 4 % paraformaldehyde and subsequently decalcified in 14 % EDTA for 12 weeks and embedded in paraffin. Sections of 5 μm were stained with tartrate−resistant acid phosphatase (TRAP; Sigma−Aldrich, St. Louis, MO, United States). Images were analyzed using Adobe Photoshop C6 software (Adobe Systems, Inc., San José, CA, United States) and ImageJ software (NIH Image, Bethesda, MD, United States). In the distal femur, the osteoclast number over bone surface area (N.Oc/BS) and density of osteocytes per trabecular bone area were identified. Osteocyte and lacunae numbers were determined in a selected trabecular bone that was also quantified by measuring the total bone area in the analysis region. Osteocyte density was calculated by dividing the number of counted cells/lacunae by the area of trabecular bone. Sections of the femur were also stained with Masson's Trichrome. Osteoblast number per bone perimeter (N.Oc/B·Pm) was determined in the distal femur by using ImageJ software (NIH Image, Bethesda, MD, United States). Osteoblast number and the trabecular bone perimeter were quantified in the analysis region. Osteoblast density was calculated by dividing the number of counted cells (#)/the perimeter of trabecular bone (mm).

2.3. Statistical analysis

Statistical analysis of the data was executed with the support of the software GraphPad Prism 8.0 (GraphPad Software, Inc., San Diego, CA). Comparisons among the groups were performed by analysis of variance (ANOVA), followed by post hoc comparisons by the Tukey test. Differences between independent variables of two groups were accessed by the Student's *t*-test or Mann–Whitney test according to the presence or absence of a normal distribution. Proportion among groups was compared, using the Fisher's test. Significance was assumed at $P < 0.05$.

3. Results

3.1. Weight

Androgenized OVX rats were heavier than rats in other groups at Day 180 of life. The weight (mean ± SD) of androgenized rats was 377.8 ± 37.2 g versus 289.5 ± 9.75 g for Control OVX rats, 306.6 ± 10.48 g for Androgenized SHAM rats and 289.9 ± 11,64 g for Control SHAM rats (ANOVA $p = 0.01$). The weight (mean ± SD) of Androgenized SHAM rats was 306.6 ± 10.4 g versus Control SHAM of 289.9 ± 11.64 g (Student's *t*-test $p = 0.004$).

3.2. Estrous cycles and ovarian histology

Evidence of chronic anovulation was identified in all Androgenized groups (Supplemental Fig. 1). The rats in the SHAM Control group exhibited all phases of estrus that were different from those of rats in the SHAM androgenized group. We also observed a significant reduction in the number of corpora lutea in Androgenized SHAM rats, mean ± SEM of 1.51 ± 0.57 versus SHAM Control rats 5.16 ± 1.83 (Student *t*-test $p = 0.002$) (Supplemental Fig. 2). The number of healthy follicles was reduced in Androgenized SHAM rats, mean ± SEM of 3.49 ± 0.89, in comparison to Control SHAM rats, 7.6 ± 2.26, but the difference did not reach statistical significance (Student *t*-test $p = 0.006$).

3.3. Femur size and weight

At Day 180 of life, the Androgenized OVX group exhibited an increased femur weight (mean ± SD) of 1.33 ± 0.24 g compared with the Control OVX, Control SHAM and Androgen SHAM groups, which had weights of 1.17 ± 0.17 g, 1.12 ± 0.11 g and 1.13 ± 0.08, respectively (ANOVA p = 0.04) (Fig. 1A). Femoral length was significantly elevated in the Androgenized OVX group in comparison to the other groups (ANOVA 0.01), as shown in Fig. 1B.

3.4. Micro-CT

3.4.1. Femur Micro-CT

A schematic figure representing micro-CT images of the spine and femur of each studied group is shown in Fig. 2A and B. In Androgenized SHAM rats, a clear increase in the femoral trabecular bone occurred that decreased considerably after oophorectomy (Fig. 2C). This trabecular loss was less severe in the spine of Androgenized OVX rats (Fig. 2D). Androgenized SHAM rats showed a strong increase in many micro-CT trabecular bone parameters. For example, BMD (Fig. 3A), BV (Fig. 3B), BV/BT (Fig. 3C), and trabecular thickness (Fig. 3D) were significantly elevated, while trabecular separation (Fig. 3F) and SMI (Fig. 3G) were decreased in Androgenized SHAM rats compared with the measures observed in Control SHAM rats. No differences were seen regarding the trabecular number (Fig. 3E) among SHAM rats. Cortical parameters (Ct.Ar/Tt. Ar) (Fig. 3I), cortical thickness (Ct.th) (Fig. 3J), and T.Pm (Fig. 3L) were diminished in Androgenized SHAM rats. These results suggested an augmentation in the trabecular bone content contrast with a reduction in the fraction of the cortical area. After ovariectomy, micro-CT parameters, such as the bone mineral density (BMD) (Fig. 3A), (BV/BT) (Fig. 3C), (Tb.th) (Fig. 3D), and (tb.n) (Fig. 3E) decreased, and the trabecular separation (Tb.sp) (Fig. 3F) increased in both Androgenized and Control rats. With exceptions of the trabecular thickness (Tb.th) (Fig. 3D), BV/BT (Fig. 3C) and BMD (Fig. 3C), a reduction in trabecular bone parameters after ovariectomy was proportional in control and androgenized rats. The cortical area (Tt.

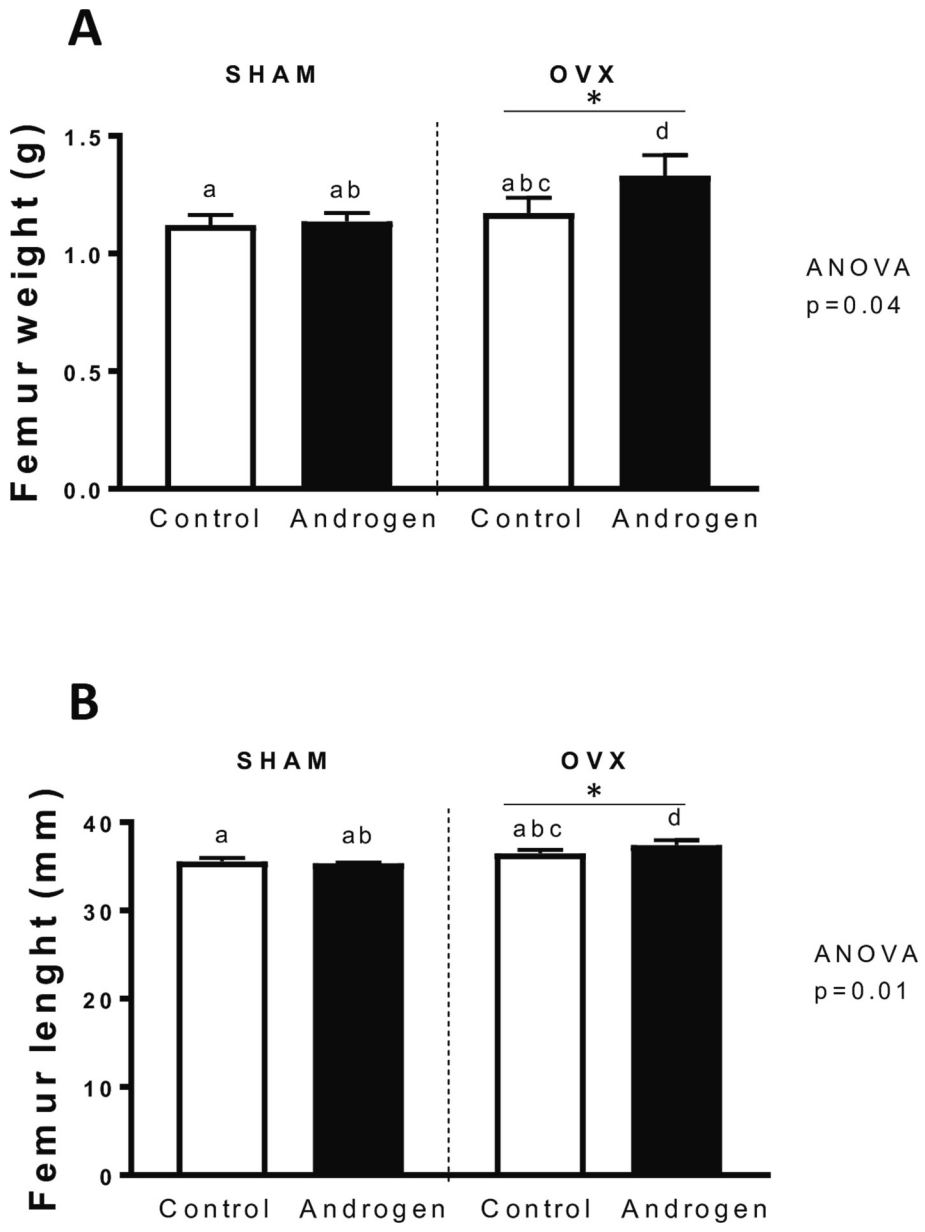

Fig. 1. Femur weight and length. Androgen+ OVX rats show an increase in femur weight (A) and length (B) after ovariectomy; no differences were observed in SHAM rats. Data are represented as mean ± SEM. Differences between Androgenized versus Control groups are represented by * when $p < 0.05$.

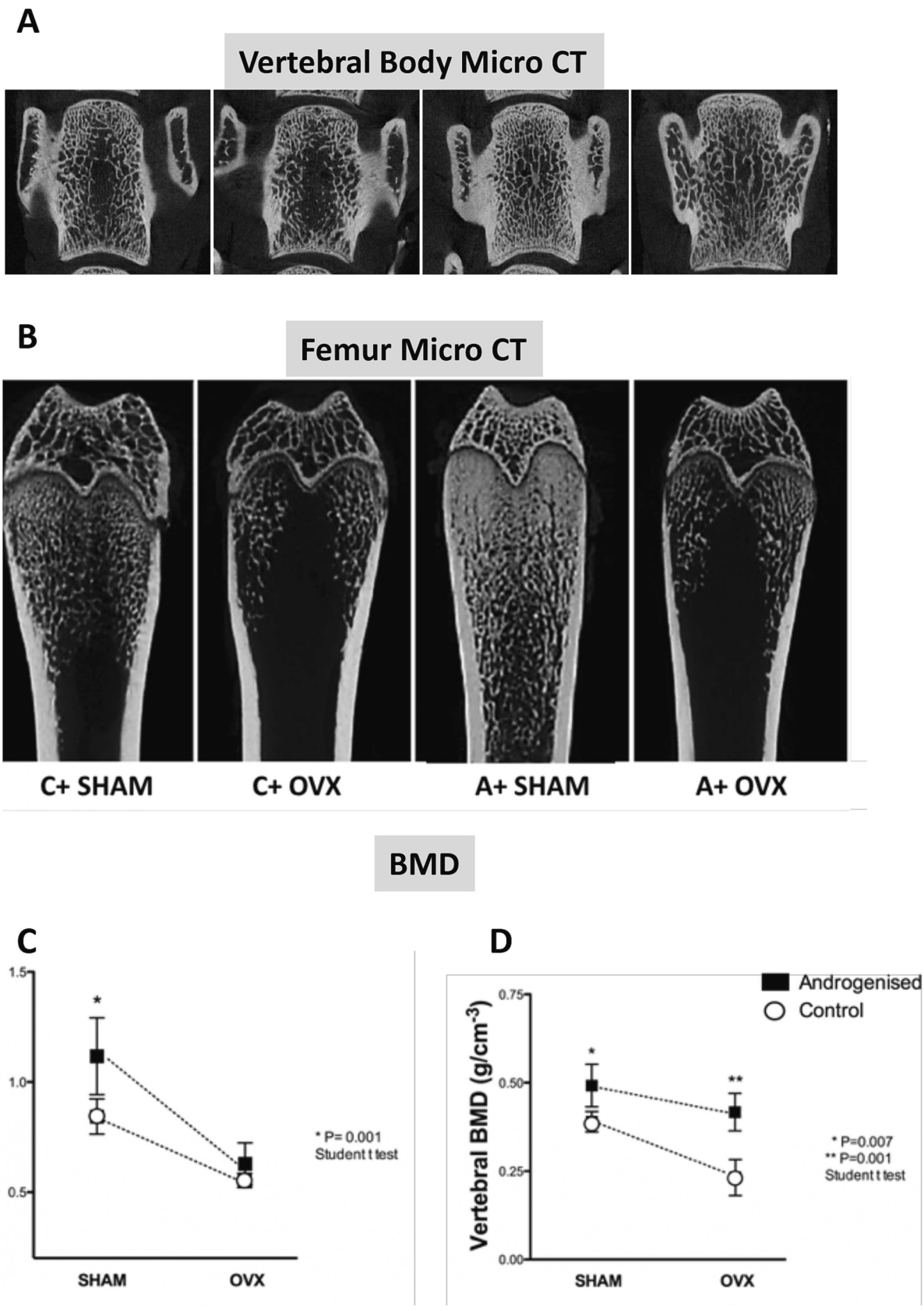

Fig. 2. Representative micro-CT images of the distal femur and spine of the four main groups of the study and the values of bone mineral density (BMD) at both sites. Androgenized SHAM (A+ SHAM) rats exhibited a clear increase in the trabecular bone in the femur and spine in comparison to Control SHAM (C+ SHAM). After ovariectomy, the vertebral BMD remained increased in androgenized rats, while the femoral BMD was similar between the A+ OVX and C+ OVX groups. Connecting lines are a simple projection of the corresponding values between control and androgenized rats not corresponding to a mathematical equation. Data are represented as mean ± SEM. Differences between Androgenized versus Control groups are represented by * when $p < 0.05$.

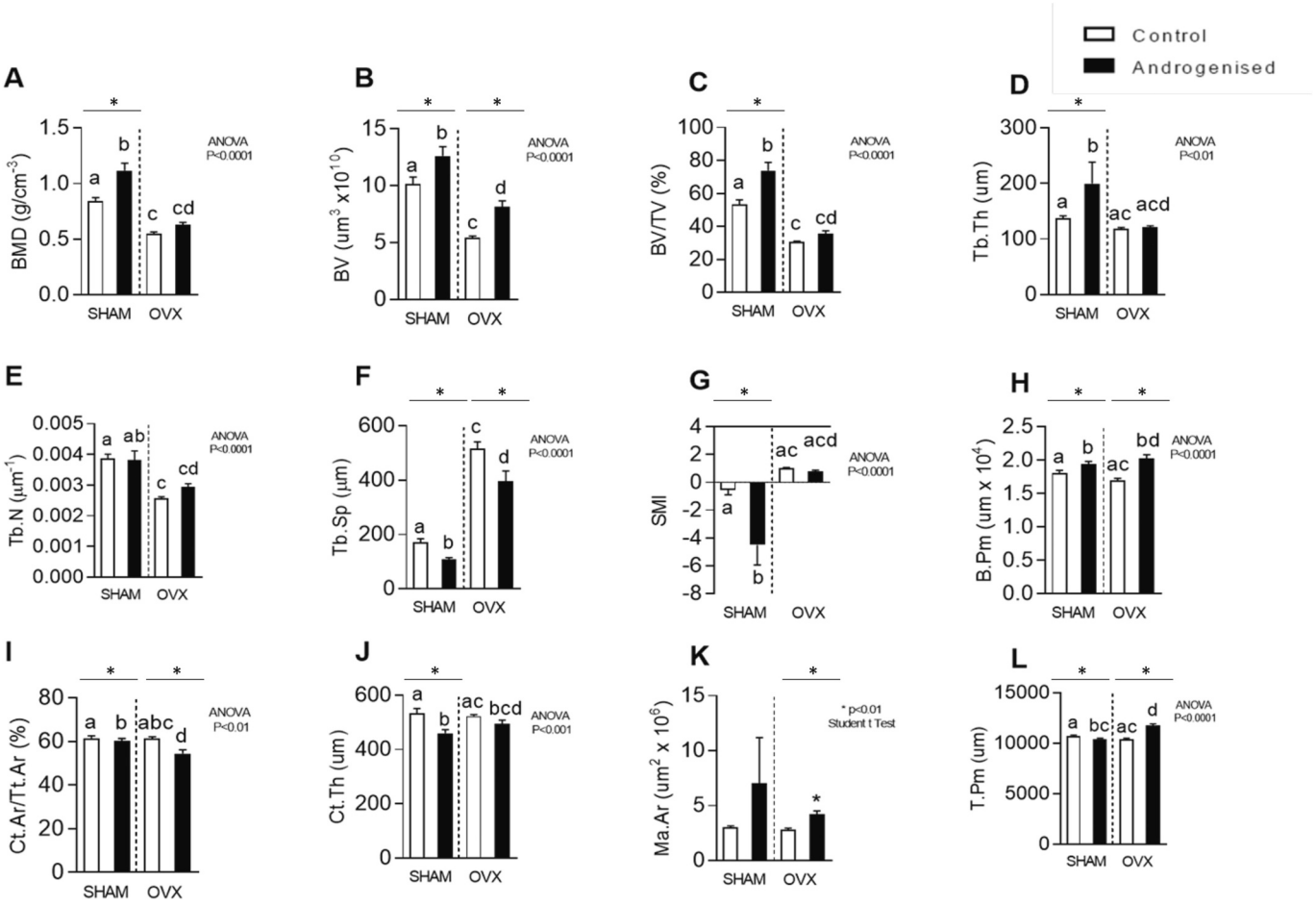

Fig. 3. Micro-CT: analysis of the trabecular and cortical bones of the femur. (A) bone mineral density (BMD g/cm); (B) bone volume (BV mm); (C) bone volume/total volume ratio (BV/TV%); (D) trabecular thickness (Tb.Th mm); (E) trabecular number (Tb.n mm); (F) trabecular separation (Tb.sp. mm); and (G) the structure model index (SMI); (H)B·Pm (bone perimeter); (I)Tt.Ar/Ct.Ar (fraction of cortical area %); (J) Ct.Th (cortical thickness mm)(K) Ma.Ar (medullary area);(L) T.Pm (total perimeter). Differences between Androgenized versus Control groups are represented by * when $p < 0.05$.

Ar/Ct.Ar) (Fig. 3I) continued to decrease in the Androgenized OVX rats, while the cortical thickness (Ct.th) (Fig. 3J) was approximately the same as that of the controls (Fig. 3I). The bone perimeter was significantly increased in both androgenized groups (SHAM and OVX) compared with its respective controls (Fig. 3L).

3.4.2. *Spine Micro-CT*

Changes in the vertebral micro-CT were also based on the elevation of trabecular bone. BMD (Figs. 2D, 4A), BV (Fig. 4B), and BV/BT (Fig. 4C) were increased in Androgenized SHAM and Androgenized OVX rats compared with that in Control SHAM and OVX rats. Similar to the results noted in the femur, we observed an increase in the trabecular number (Fig. 4E) and a reduction in the trabecular separation (Fig. 4F), but the trabecular thickness (Fig. 4D) was not different between the androgenized OVX and Control OVX groups. SMI was significantly reduced in the androgenized groups (Fig. 4G).

3.4.3. *P1NP and CTX*

At Day 180 of life, Androgenized SHAM rats showed levels of circulating P1NP comparable to those of Control SHAM rats (Fig. 5A). In Androgenized SHAM rats, the mean (+ SD) for P1NP was 51.91 ± 12.85 ng/ml versus Control SHAM 35.57 ± 17.5 ng/ml. However, after ovariectomy, P1NP levels decreased significantly in the Androgenized OVX group in comparison to Control OVX rats. We also observed an increase in P1NP levels in ovariectomized rats compared with SHAM rats, reflecting higher bone turnover. The levels of CTX, a marker of bone resorption, were significantly reduced in androgenized rats (SHAM group) versus controls, but both groups were similar after ovariectomy (Fig. 5B).

3.4.4. *Mechanical test*

A mechanical test was performed to establish the strength and stiffness of the femurs of control and androgenized rats. As shown in Fig. 6A, Androgenized SHAM rats presented a significant reduction in femur bone strength. The bone stiffness did not demonstrate a significant reduction (Fig. 6B).

3.4.5. *Osteoblast and osteoclast number*

Results from this analysis included a limited number of samples (from 3 to 6 in each group, as some were discarded for being considered not suitable). As shown in Fig. 7, at day 180 of life, an increased number of osteoclast in both Androgenized groups compared to its controls(7C). However, while a consistent decrease in the number of osteocytes(7A) and osteoblasts(7B) was identified in Androgenized SHAM groups, no differences in these parameters were shown in Androgenized OVX versus Control OVX (Fig. 7A and B).

4. Discussion

The present study combined a neonatal testosterone-treated rat and an experimental osteoporosis model to explore the impact of androgens on bone markers, micro-CT parameters, in adulthood (Day 100) and the

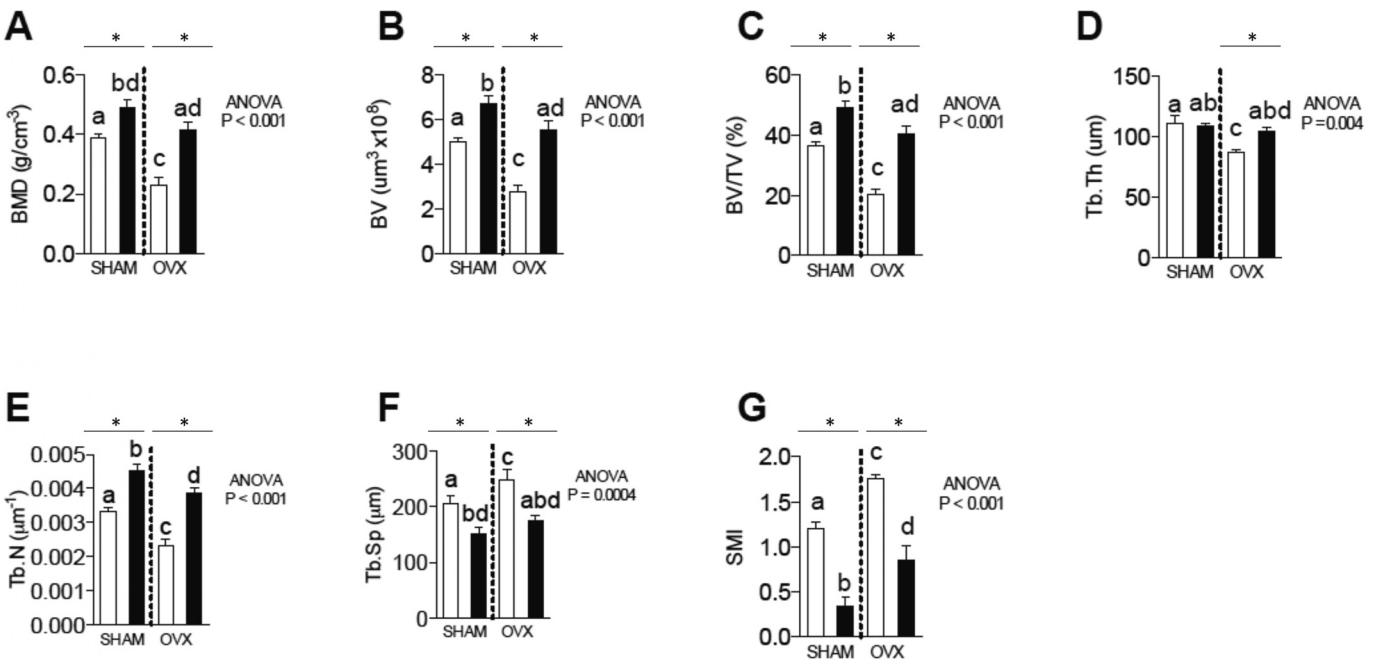

Fig. 4. Micro-CT: analysis of the spine trabecular bone. (A) bone mineral density (BMD g/cm); (B) bone volume (BV mm); (C) bone volume/total volume ratio (BV/TV%); (D) trabecular thickness (Tb.Th mm); (E) trabecular number (Tb.n mm); (F) trabecular separation (Tb.sp. mm); and (G) the structure model index (SMI). Most of these variables were affected by neonatal androgenization and influenced by oophorectomy. Differences between Androgenized versus Control groups are represented by * when $p < 0.05$.

performance of mechanical strength tests measured at 180 days of life.

As shown, two main abnormalities were observed in Androgenized SHAM rat bones. First, Androgenized SHAM rats exhibited a markedly increased trabecular bone mass, consistent with findings from previous reports (Tamura et al., 2005; Turner et al., 1990; Mujica et al., 2021). In the study of Tamura et al., Sprague–Dawley rats were subjected to TP treatment at day nine of life, and the bone parameters (bone densitometry and histomorphometry) were assessed at four months of age (Tamura et al., 2005). These androgenized rats showed a marked elevation of the BMD of the tibia with higher BV/BT of the tibia at histomorphometry analysis and lower bone turnover, though there were no results characterizing the cortical area and thickness. We previously explored micro-CT bone changes in Wistar rats at Day 110 of life treated with testosterone propionate at Day 2 of life, observing an increased trabecular bone of androgenized rats in relation to controls (Mujica et al., 2021). Our study identified reduced bone resorption (CTX) as a possible mechanism favoring the increased trabecular bone in Androgenized SHAM rats (most circulating CTX originates from trabecular bone rather than cortical bone). Testosterone may also enhance trabecular bone, reducing bone resorption; once the rat model used in our study (1.25 mg of testosterone propionate) presents hyperandrogenism as one of the main characteristics, this could be a conceivable mechanism involved in the enhancement of trabecular bone (Yarrow et al., 2008). Looking into the micro CT parameters, we noteddifferences between the femur and spine. In the femur, the trabecular thickness was reduced in Androgenized OVX versus Androgenized SHAM, but no difference was identified between Control rats. In the spine, we observe the opposite: there was a significant reduction in the trabecular thickness in Control OVX versus Control SHAM, but not in Androgenized OVX rats against Androgenized SHAM. This tendency reflects the total BMD before and after oophorectomy, as shown in Fig. 2. The second abnormality identified in these androgenized rats was a reduction in the cortical thickness associated with increased cortical fragility at Day 180 of life. This unexpected finding occurred against initial expectations of higher bone strength since continued supraphysiological replacement of androgens may cause increases in cortical thickness, cortical area and mechanical strength (Yarrow et al., 2008; Stuermer et al., 2009). Because our study is the first to perform mechanical tests on an animal model of PCOS, we do not have comparisons to be established. One potential element that could contribute to the reduction of the cortical thickness and the cortical area is insulin resistance, which was verified in this rat model (TP 1.25 mg neonatal) and previously published by our group (Serrano Mujica et al., 2021). Evidence in humans corroborates the role of insulin in decreasing cortical thickness (and a trend to elevate trabecular bone) suggested by its reduction in type 2 diabetes, as reported by the cohorts of Framingham, the SWAN study and the Hertfordshire Cohort Study (Samelson et al., 2018; Yu et al., 2015; Paccou et al., 2016). Other elements not addressed in our study that would support a reduction in bone strength would be the cortical porosity, which is associated with an increased risk of bone fractures in women (Samelson et al., 2018). Abnormalities in osteocytic perilacunar/canalicular turnover have also been demonstrated in experimental type 2 diabetes (Pei et al., 2021). Changes in the osteoid are especially important because they may affect bone quality and increase fragility and risk of fractures despite the presence of a normal bone mass densitometry which is common in type 2 diabetes (Vestergaard, 2007).

Our study also analyzed, for the first time, the features of Androgenized (PCOS) and Control rat bones following oophorectomy. Curiously, after ovary removal and reduction of BMD in both OVX groups, differences in the cortical and trabecular bone mass disappeared over time in the femur, but not in the spine. This suggests that femoral changes in Androgenized SHAM rats are more dependent or influenced by the hormonal milieu promoted by the developmental process. Except for the number of osteoclasts, which increased in both Androgenized groups, Androgenized OVX rats did not differ from Control OVX rats in terms of osteoblasts and osteocytes. However, it is not possible to say if this was the main factor for the mechanical test of Androgenized OVX being similar to Control OVX.

Although we did not measure androgens directly in this study, previous reports with a similar PCOS rat (testosterone propionate 1.25 mg s. c. from Days 2–5 after birth) showed an increased levels of testosterone

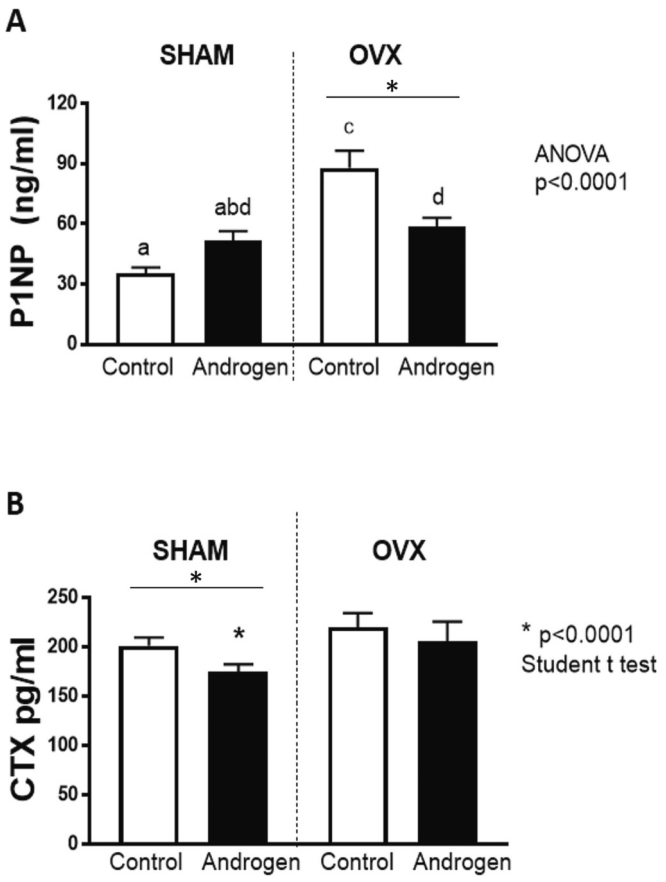

Fig. 5. Levels of P1NP and CTX. (A) P1NP, a marker of bone formation, was decreased in Androgen +OVX rats in comparison to controls. No statistically significant differences were observed between Androgen+ SHAM animals and the Control+ SHAM animals. In contrast, (B) the levels of CTX, a marker of bone resorption, were decreased in Androgen + SHAM rats ($p < 0.0001$). A similar CTX was observed in both groups after ovariectomy (Control +OVX and Androgenized + OVX). Data are represented as mean ± SEM. Differences between Androgenized versus Control groups are represented by * when $p < 0.05$.

at Day 90 of life (Anzai et al., 2017; Marcondes et al., 2015), opening the possibility of a direct or indirect role of testosterone in bone formation and resorption. The assessment of LH levels was not realized. That is also another limitation, since the maturity of the hypothalamic-gonadal axis may be affected by steroids. In the study of Pinnila et al., rats treated with 1.25 mg of Testosterone propionate in the five days of birth exhibited a reduction in LH levels 14 days of oophorectomy executed at day 90 of life, reflecting some degree of insensibility or immaturity of the gonadal axis in (Pinilla et al., 2002). However, is not possible to acknowledge whether this expected condition may have interfered directly or indirectly with the observed endpoints in our study.

Excessive reactive oxygen species (ROS) production, signalizing an activated REDOX state, affects the formation of osteoblasts and impairs their activity, viability, proliferation, and apoptosis. The reduction in the osteoblastic number and functionality would lead to lower bone formation. There is also an activation of osteoclastogenesis and differentiation by oxidants and inflammatory mediators. All these changes result in altered bone architecture and impaired bone acquisition or bone loss (Iantomasi et al., 2023; Domazetovic et al., 2017).

In our study, oophorectomy causes a reduction in oxidative stress markers in this rat model of PCOS, such as a decrease in the total oxidant status (TOS) (Serrano Mujica et al., 2021), which is also expected to ameliorate bone losses.

We observed an increased gain in weight in Androgenised OVX rats. This could be explained as a combination of factors since both androgenized groups in our study were heavier than controls, which agrees with some studies of neonatal androgenization using TP (Tyndall et al., 2012), although there is not a consensus (Walters et al., 2012). Moreover, ovariectomy has been related to weight gain in rats. An increase in weight after oophorectomy has been linked by some authors to changes in estrogen receptors at the arcuate, paraventricular nucleus, and dorsal vagal complex (Burch et al., 2021). According to the work of Nebot et al., an increased length of the femur (but not the tibia) was reported in Sprague Dawley rats submitted to a high fat diet developing obesity (Nebot et al., 2022).

Some strengths of our study were related to the extensive evaluation of bone features, including micro-CT of the femur and spine, mechanical tests, and bone markers, all executed by blinded examiners. Limitations of our study occurred and were based on the lack of a complete hormone profile, bone mediators, and inflammation markers.

One important aspect is the discussion about the PCOS rat model employed. The current animal model in this study was reasonable well-characterized in the literature by anovulation, polycystic ovaries, dyslipidemia, hyperandrogenism, and insulin resistance (Anzai et al., 2017; Marcondes et al., 2015; Serrano Mujica et al., 2021; Ota et al., 1983; Pinilla et al., 2002).Therefore, there are reasons to believe that similar changes that occur in this model may be similar to other PCOS rat models (e.g. letrozole-induced).

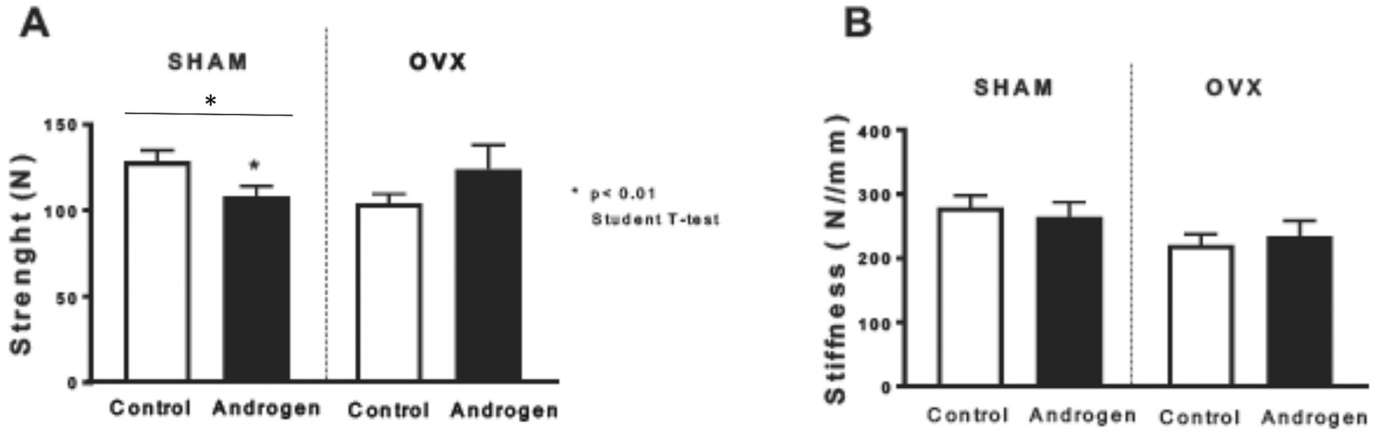

Fig. 6. Mechanical test of the femur: analysis of the strength and stiffness. (A) Androgen+ SHAM rats presented a significant decrease in the strength of the bone in comparison to controls. This difference disappeared after ovariectomy. (B) Stiffness was similar among groups. Data are represented as mean ± SEM. Differences between Androgenized versus Control groups are represented by * when $p < 0.05$.

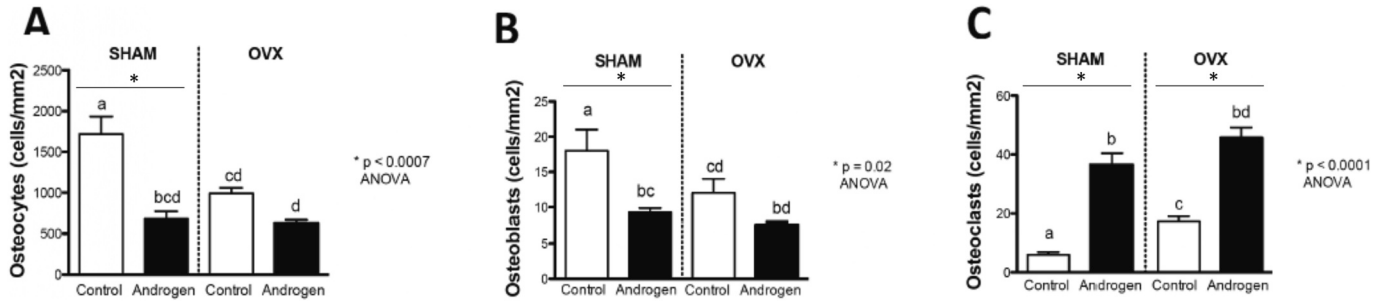

Fig. 7. Identification of osteocytes, osteoblasts, and osteoclast in the femur.
The histological identification of bone sections stained with tartarate-resistant acid phosphatase (TRAP). (A) density of osteocytes per area of trabecular bone (cells/mm2).(B) density of osteoblasts per area of trabecular bone (cells/mm^2).(C) osteoclast number over bone surface area (N.Oc/Bs). Differences between Androgenized versus Control groups are represented by * when $p < 0.05$.

5. Conclusion

In conclusion, the results from this study suggest that neonatal androgenization leads to bone changes in adult life characterized by a reduction in the cortical area, cortical thickness and femoral bone strength and a paradoxical increase in the trabecular bone mass. Ovariectomy in the androgenized OVX group limited the progression rate of cortical bone loss, resulting in a relative improvement in bone resistance in the androgenized OVX group. Future studies using different species of animal PCOS models and monitoring bone changes from the beginning of the androgenization process will help to clarify the development of abnormalities described in our report.

Supplementary data to this article can be found online at https://doi.org/10.1016/j.bonr.2023.101710.

Funding

This research did not receive any specific grant from funding agencies.

CRediT authorship contribution statement

Lady Katerine Serrano Mujica: Methodology, Investigation, Data curation. **Carolina dos Santos Amaral:** Investigation, Data curation. **Fernanda Soldatelli Valente:** Investigation. **Ligia Gomes Miyazato:** Investigation. **Soraia Macari:** Investigation, Formal analysis. **Tarcília Aparecida da Silva:** Investigation, Formal analysis. **Breno Rocha Barrioni:** Investigation. **Bruna Leonel Carlos:** Investigation. **Guilherme Jafroni Alves Silva:** Investigation. **Antônio Carlos Shimano:** Resources, Methodology, Investigation. **Alfredo Quites Antoniazzi:** Resources, Project administration, Funding acquisition. **Melissa Orlandin Premaor:** Writing – original draft, Formal analysis. **Fabio Vasconcellos Comim:** Writing – original draft, Supervision, Project administration, Methodology, Funding acquisition, Formal analysis, Conceptualization.

Declaration of competing interest

The authors declare that they have no known competing financial interests or personal relationships that could have appeared to influence the work reported in this paper.

Data availability statement

The datasets for this study can be found in the Figshare repository (figshare https://doi.org/10.6084/m9.figshare.17088803).

Acknowledgements

We would like to thank Professor Carlos Fernando Mello from the Postgraduate Program in Pharmacology (UFSM) and the Animal Care Facility (UFSM) for the support for animal breeding and manipulation.

References

Anzai, A., et al., 2017. Impaired branched-chain amino acid metabolism may underlie the nonalcoholic fatty liver disease-like pathology of neonatal testosterone-treated female rats. Sci. Rep. 7 (1), 13167.
Burch, K.E., et al., 2021. Relationship between circulating metabolic hormones and their central receptors during Ovariectomy-induced weight gain in rats. Front. Physiol. 12, 800266.
Domazetovic, V., et al., 2017. Oxidative stress in bone remodeling: role of antioxidants. Clin. Cases Miner. Bone Metab. 14 (2), 209–216.
Iantomasi, T., et al., 2023. Oxidative stress and inflammation in osteoporosis: molecular mechanisms involved and the relationship with microRNAs. Int. J. Mol. Sci. 24 (4).
Kalyan, S., et al., 2017. Competing factors link to bone health in polycystic ovary syndrome: chronic low-grade inflammation takes a toll. Sci. Rep. 7 (1), 3432.
Karadag, C., Yoldemir, T., Gogas Yavuz, D., 2017. Determinants of low bone mineral density in premenopausal polycystic ovary syndrome patients. Gynecol. Endocrinol. 33 (3), 234–237.
Kassanos, D., et al., 2010. Augmentation of cortical bone mineral density in women with polycystic ovary syndrome: a peripheral quantitative computed tomography (pQCT) study. Hum. Reprod. 25 (8), 2107–2114.
Katulski, K., et al., 2014. Bone mineral density in women with polycystic ovary syndrome. J. Endocrinol. Investig. 37 (12), 1219–1224.
Macari, S., et al., 2015. Oestrogen regulates bone resorption and cytokine production in the maxillae of female mice. Arch. Oral Biol. 60 (2), 333–341.
Marcondes, R.R., et al., 2015. Differences in neonatal exposure to estradiol or testosterone on ovarian function and hormonal levels. Gen. Comp. Endocrinol. 212, 28–33.
McCartney Ch, R., Marshall, J.C., 2016. Polycystic ovary syndrome. N. Engl. J. Med. 375 (14), 1398–1399.
Montalvany-Antonucci, C.C., et al., 2018. High-fat diet disrupts bone remodeling by inducing local and systemic alterations. J. Nutr. Biochem. 59, 93–103.
Monteiro, L.O., et al., 2016. Effect of treatment with simvastatin on bone microarchitecture of the femoral head in an osteoporosis animal model. Microsc. Res. Tech. 79 (8), 684–690.
Mujica, L.K.S., et al., 2021. Trabecular bone is increased in a rat model of polycystic ovary syndrome. Exp. Clin. Endocrinol. Diabetes 129 (10), 757–761.
Nebot, E., et al., 2022. Combination of caloric restriction and a mixed training protocol as an effective strategy to counteract the deleterious effects in trabecular bone microarchitecture caused by a diet-induced obesity in Sprague Dawley rats. Nutrients 14 (18).
Ota, H., Fukushima, M., Maki, M., 1983. Endocrinological and histological aspects of the process of polycystic ovary formation in the rat treated with testosterone propionate. Tohoku J. Exp. Med. 140 (2), 121–131.
Paccou, J., et al., 2016. Bone microarchitecture in men and women with diabetes: the importance of cortical porosity. Calcif. Tissue Int. 98 (5), 465–473.
Padmanabhan, V., Veiga-Lopez, A., 2013. Animal models of the polycystic ovary syndrome phenotype. Steroids 78 (8), 734–740.
Pei, Q., et al., 2021. A potential participant in type 2 diabetes bone fragility: TIMP-1 at sites of osteocyte lacunar-Canalicular system. Diabetes Metab. Syndr. Obes. 14, 4903–4909.
Pinilla, L., et al., 2002. Comparative effects of testosterone propionate, oestradiol benzoate, ICI 182,780, tamoxifen and raloxifene on hypothalamic differentiation in the female rat. J. Endocrinol. 172 (3), 441–448.
Piovezan, J.M., Premaor, M.O., Comim, F.V., 2019. Negative impact of polycystic ovary syndrome on bone health: a systematic review and meta-analysis. Hum. Reprod. Update 25 (5), 633–645.

Rubin, K.H., et al., 2016. Fracture risk is decreased in women with polycystic ovary syndrome: a register-based and population-based cohort study. J. Bone Miner. Res. 31 (4), 709–717.
Samelson, E.J., et al., 2018. Diabetes and deficits in cortical bone density, microarchitecture, and bone size: Framingham HR-pQCT study. J. Bone Miner. Res. 33 (1), 54–62.
Schmidt, J., et al., 2012. Body composition, bone mineral density and fractures in late postmenopausal women with polycystic ovary syndrome - a long-term follow-up study. Clin. Endocrinol. 77 (2), 207–214.
Serrano Mujica, L.K., et al., 2017. The impact of postnatal leuprolide acetate treatment on reproductive characteristics in a rodent model of polycystic ovary syndrome. Mol. Cell. Endocrinol. 442, 125–133.
Serrano Mujica, L.K., et al., 2021. Ovariectomy improves metabolic and oxidative stress marker disruption in androgenized rats: possible approach to postmenopausal polycystic ovary syndrome. Metab. Syndr. Relat. Disord. 19 (5), 312–316.
Sir-Petermann, T., et al., 2016. Metabolic features across the female life span in women with PCOS. Curr. Pharm. Des. 22 (36), 5515–5525.
Stener-Victorin, E., et al., 2020. Animal models to understand the etiology and pathophysiology of polycystic ovary syndrome. Endocr. Rev. 41 (4).
Stuermer, E.K., et al., 2009. Effect of testosterone, raloxifene and estrogen replacement on the microstructure and biomechanics of metaphyseal osteoporotic bones in orchiectomized male rats. World J. Urol. 27 (4), 547–555.
Sun, J., et al., 2013. Effects of electroacupuncture of “Guanyuan” (CV 4)-“Zhongji” (CV 3) on ovarian P450 arom and P450c 17alpha expression and relevant sex hormone levels in rats with polycystic ovary syndrome. Zhen Ci Yan Jiu 38 (6), 465–472.
Tamura, N., et al., 2005. Effects of testosterone on cancellous bone, marrow adipocytes, and ovarian phenotype in a young female rat model of polycystic ovary syndrome. Fertil. Steril. 84 (Suppl. 2), 1277–1284.
Teede, H.J., et al., 2018. Recommendations from the international evidence-based guideline for the assessment and management of polycystic ovary syndrome. Hum. Reprod. 33 (9), 1602–1618.
Turner, R.T., et al., 1990. Dehydroepiandrosterone reduces cancellous bone osteopenia in ovariectomized rats. Am. J. Phys. 258 (4 Pt 1), E673–E677.
Tyndall, V., et al., 2012. Effect of androgen treatment during foetal and/or neonatal life on ovarian function in prepubertal and adult rats. Reproduction 143 (1), 21–33.
Vestergaard, P., 2007. Discrepancies in bone mineral density and fracture risk in patients with type 1 and type 2 diabetes–a meta-analysis. Osteoporos. Int. 18 (4), 427–444.
Walters, K.A., Allan, C.M., Handelsman, D.J., 2012. Rodent models for human polycystic ovary syndrome. Biol. Reprod. 86 (5), 149, 1-12.
Yanagihara, G.R., et al., 2015. Effects of long-term administration of omeprazole on bone mineral density and the mechanical properties of the bone. Rev. Bras. Ortop. 50 (2), 232–238.
Yang, H.Y., et al., 2018. Increased risk of fractures in patients with polycystic ovary syndrome: a nationwide population-based retrospective cohort study. J. Bone Miner. Metab. 36 (6), 741–748.
Yarrow, J.F., et al., 2008. Supraphysiological testosterone enanthate administration prevents bone loss and augments bone strength in gonadectomized male and female rats. Am. J. Physiol. Endocrinol. Metab. 295 (5), E1213–E1222.
Yu, E.W., et al., 2015. Defects in cortical microarchitecture among African-American women with type 2 diabetes. Osteoporos. Int. 26 (2), 673–679.